Supporting Information

Hollow Spherical Doped Carbon Catalyst Derived from Zeolitic Imidazolate Framework Nanocrystals Impregnated/Covered with Iron Phthalocyanines

Ruiping Zheng, Shijun Liao*, Sanying Hou, Xiaochang Qiao, Guanghua Wang, Lina Liu, Ting Shu, Li Du

The Key Laboratory of Fuel Cell Technology of Guangdong Province & The Key Laboratory of New Energy, School of Chemistry and Chemical Engineering, South China University of Technology, Guangzhou 510641, China

*E-mail address for corresponding author: chsjliao@scut.edu.cn   (Shijun Liao)
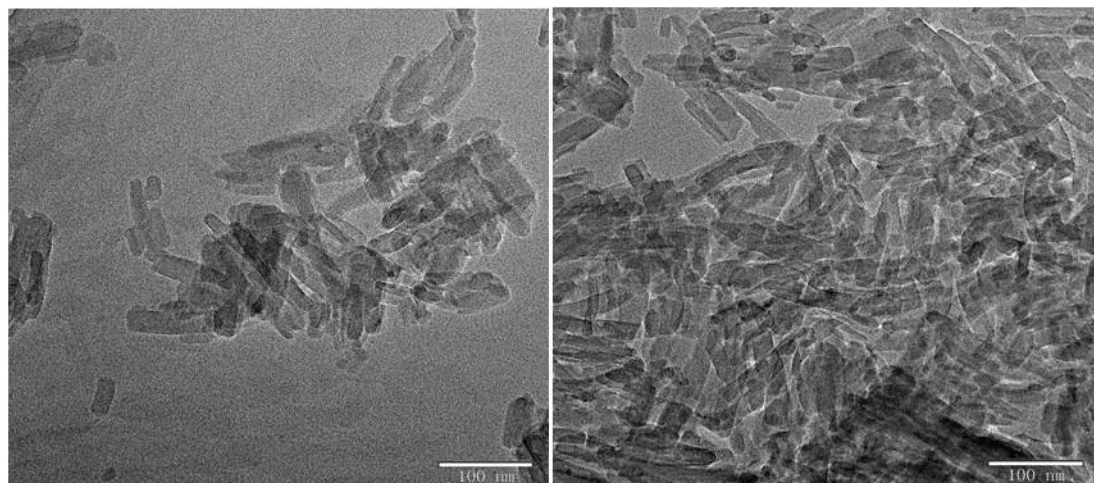

Fig. S1 TEM images of FePc.
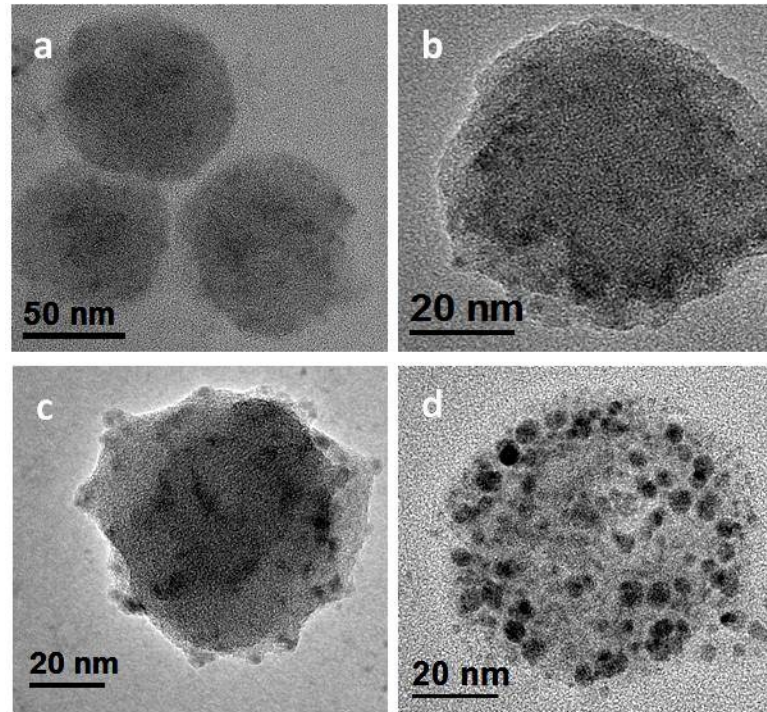
Fig. S2 TEM images of Z8Nc/FePc precursors with different Fe contents (a) 1wt%, (b) 3wt%, (c) 4wt%, (d) 5wt% Fe.

Table S1. BET surface areas, contents of C, O, N, Fe of the samples.

Samples	BET surface area $(m^2\,g^{-1})$	C content (at%)	O content (at%)	N content (at%)	Fe content (at%)
Z8Nc	1429.6	/	/	/	/
Z8Nc/FePc	384.2	/	/	/	/
C-Z8Nc-900	1010.2	79.11	5.02	7.46	0
C-Z8Nc/FePc-700	759.4	83.23	5.59	10.76	0.43
C-Z8Nc/FePc-800	911.5	83.23	6.57	9.65	0.56
C-Z8Nc/FePc-900	1237.8	88.29	5.29	5.87	0.54
C-Z8Nc/FePc-1000	1211.3	92.87	3.66	3.04	0.47

C, O, N and Fe contents were measured by XPS.
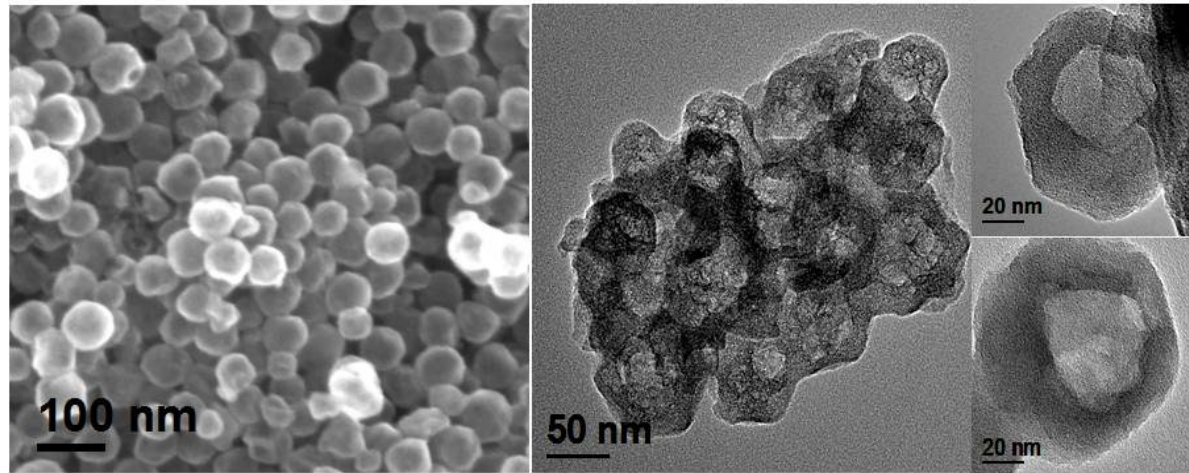
Fig. S3   SEM and TEM images of C-Z8Nc/FePc-600.
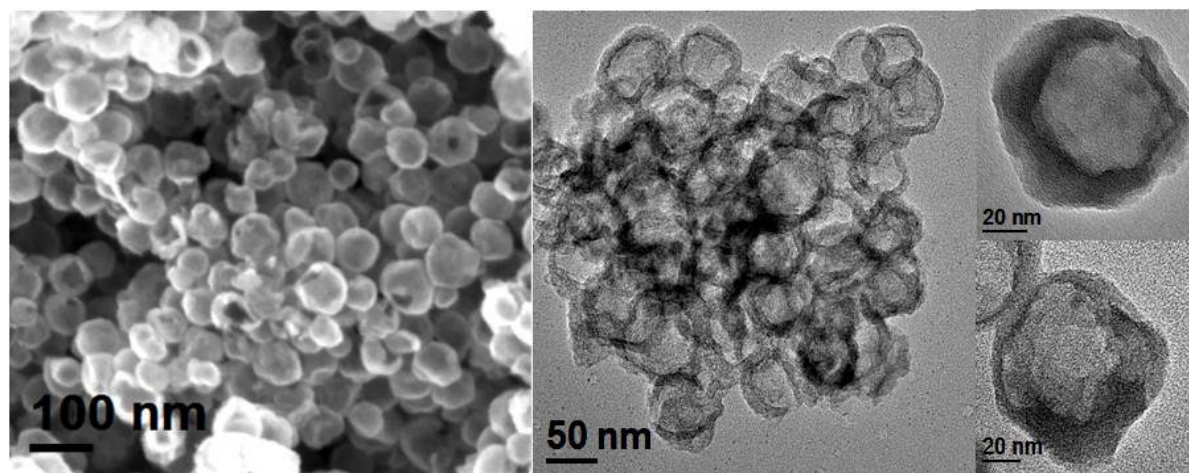
Fig. S4   SEM and TEM images of C-Z8Nc/FePc-700.
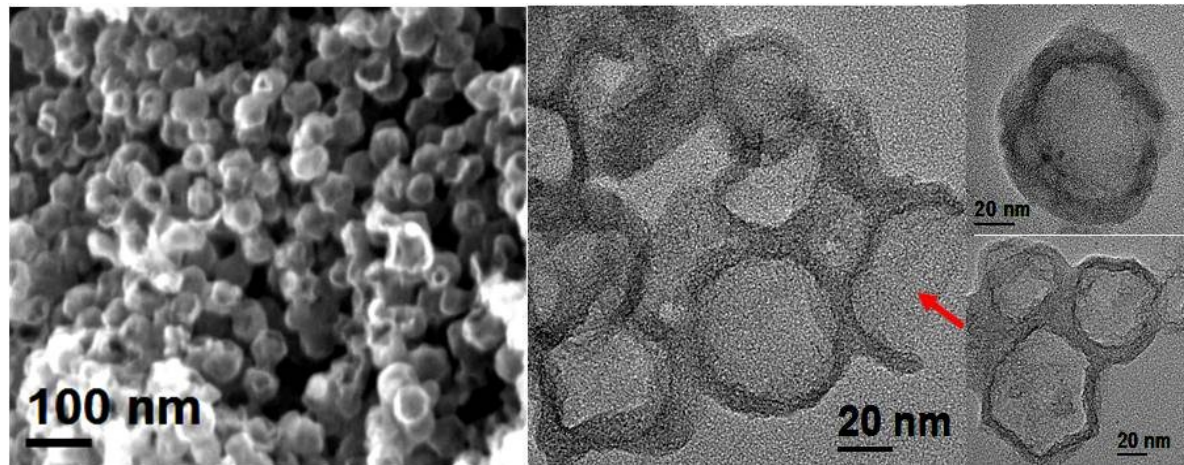
**Fig. S5**   SEM and TEM images of C-Z8Nc/FePc-800.
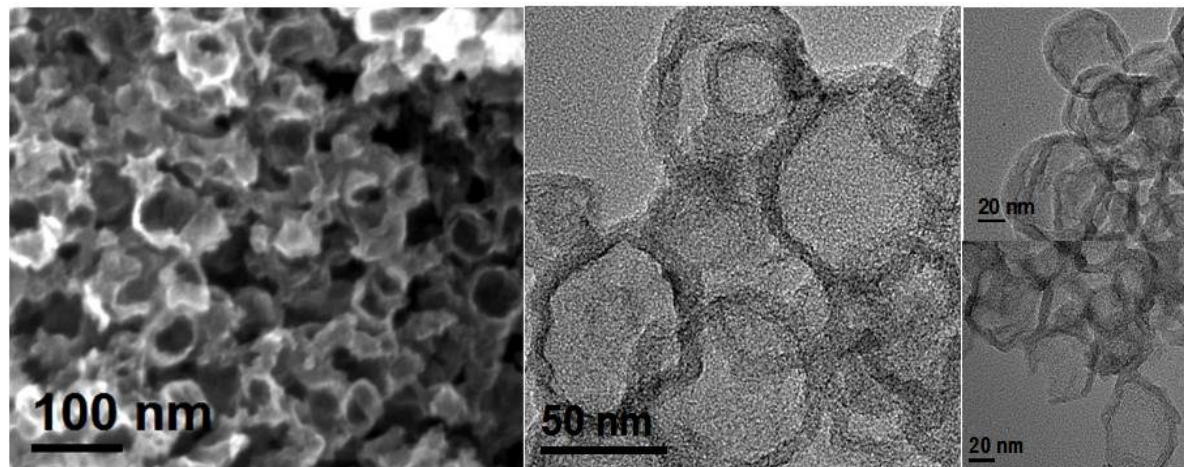
**Fig. S6**   SEM and TEM images of C-Z8Nc/FePc-1000.
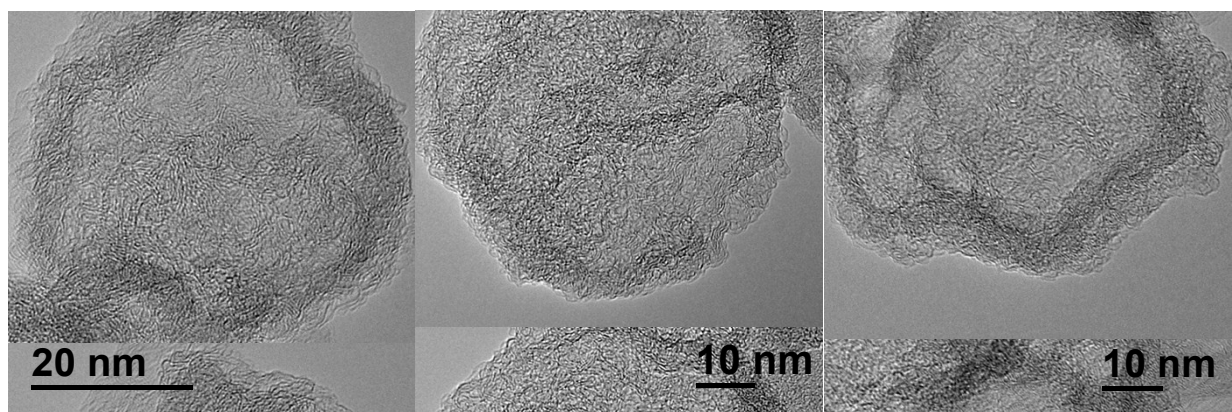
Fig. S7 High resolution TEM images of C-Z8Nc/FePc-900 after acid leaching.
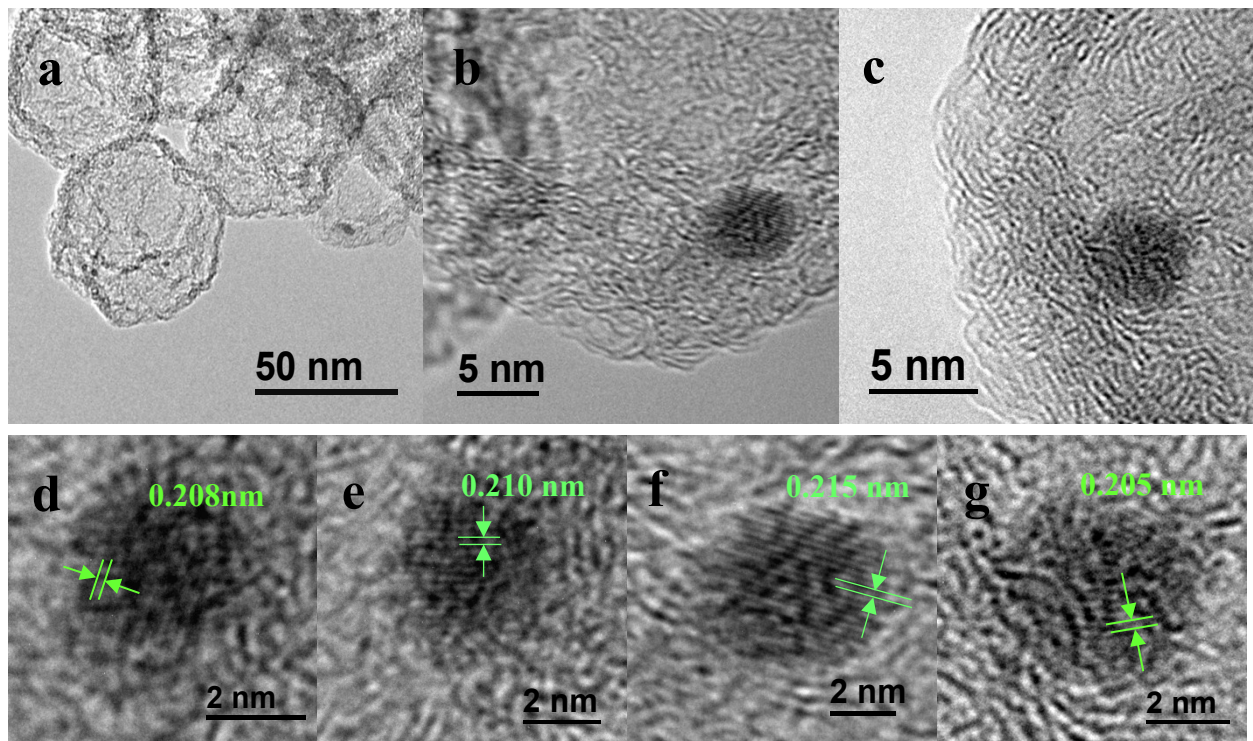
Fig. S8 High resolution TEM images of C-Z8Nc/FePc-900 before acid leaching (a-c) and high resolution TEM images of the Fe-containing nanoparticles (d-g).
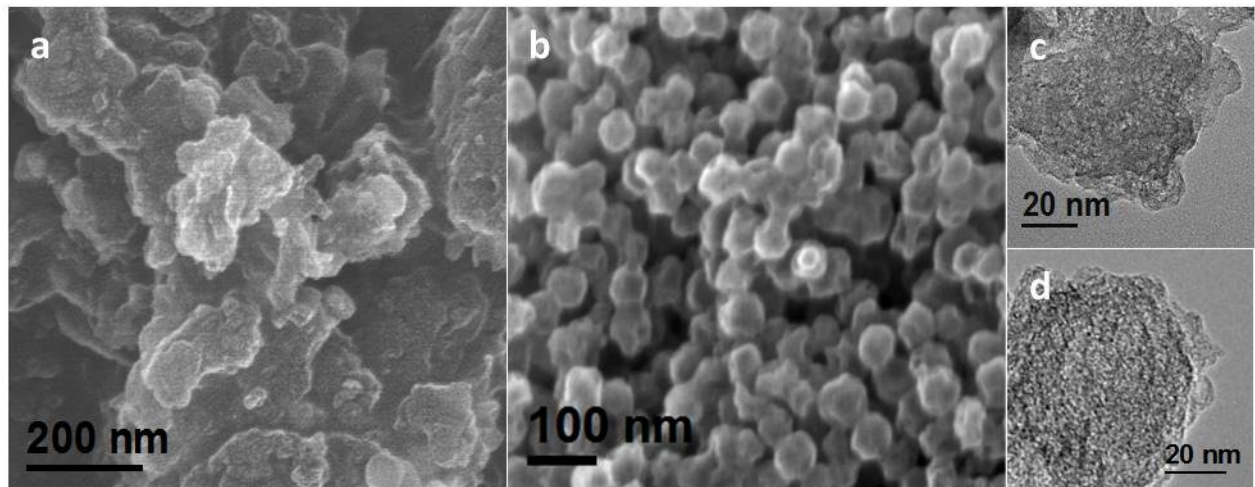
Fig. S9 (a) SEM image of C-FePc-900, (b) SEM image of C-Z8Nc-900 and (c, d) TEM images of C-Z8Nc-900.
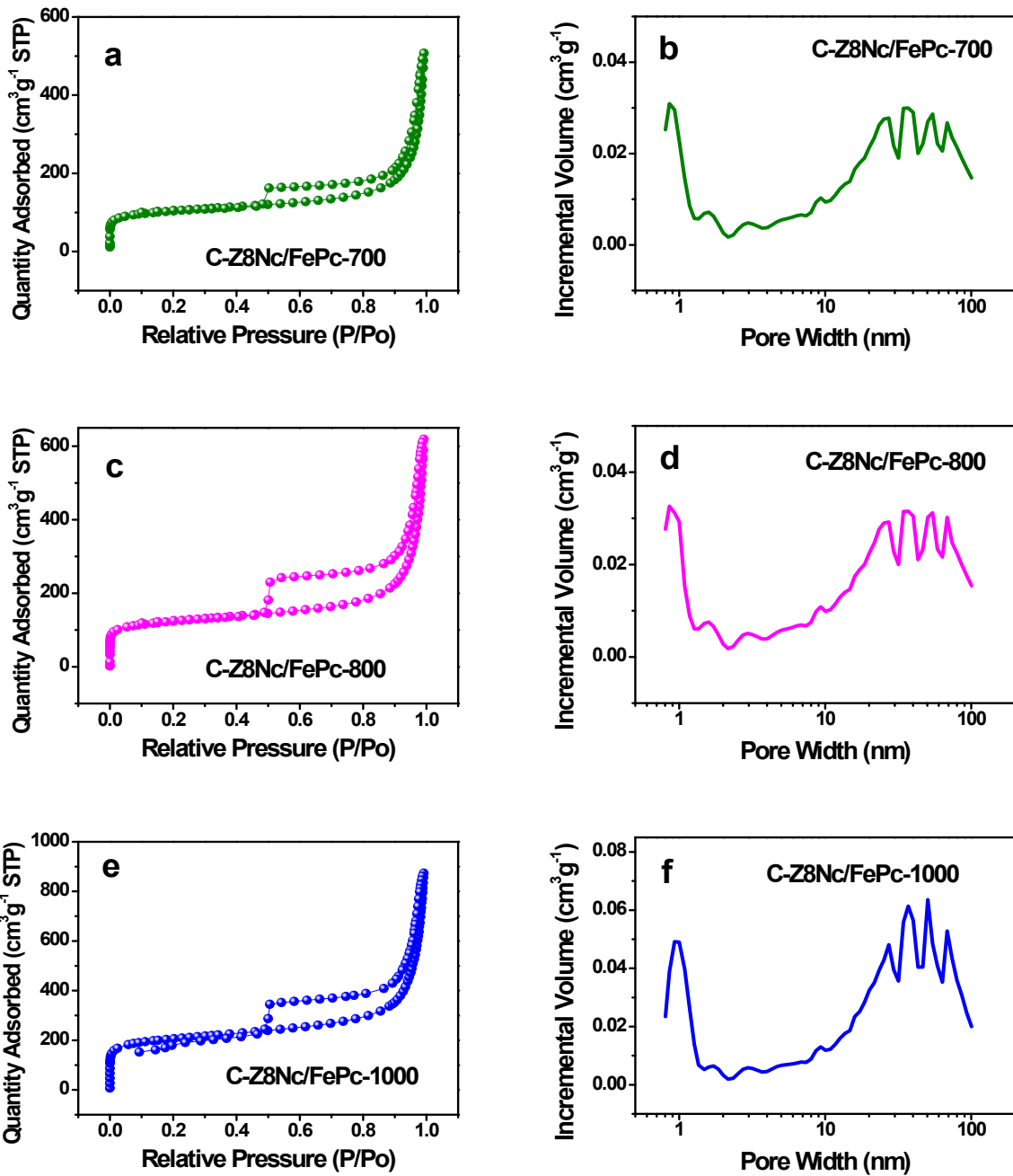
Fig. S10 N₂ adsorption and desorption isotherms and DFT pore size distributions of (a, b) C-Z8Nc/FePc-700, (c, d) C-Z8Nc/FePc-800 and (e, f) C-Z8Nc/FePc-1000.
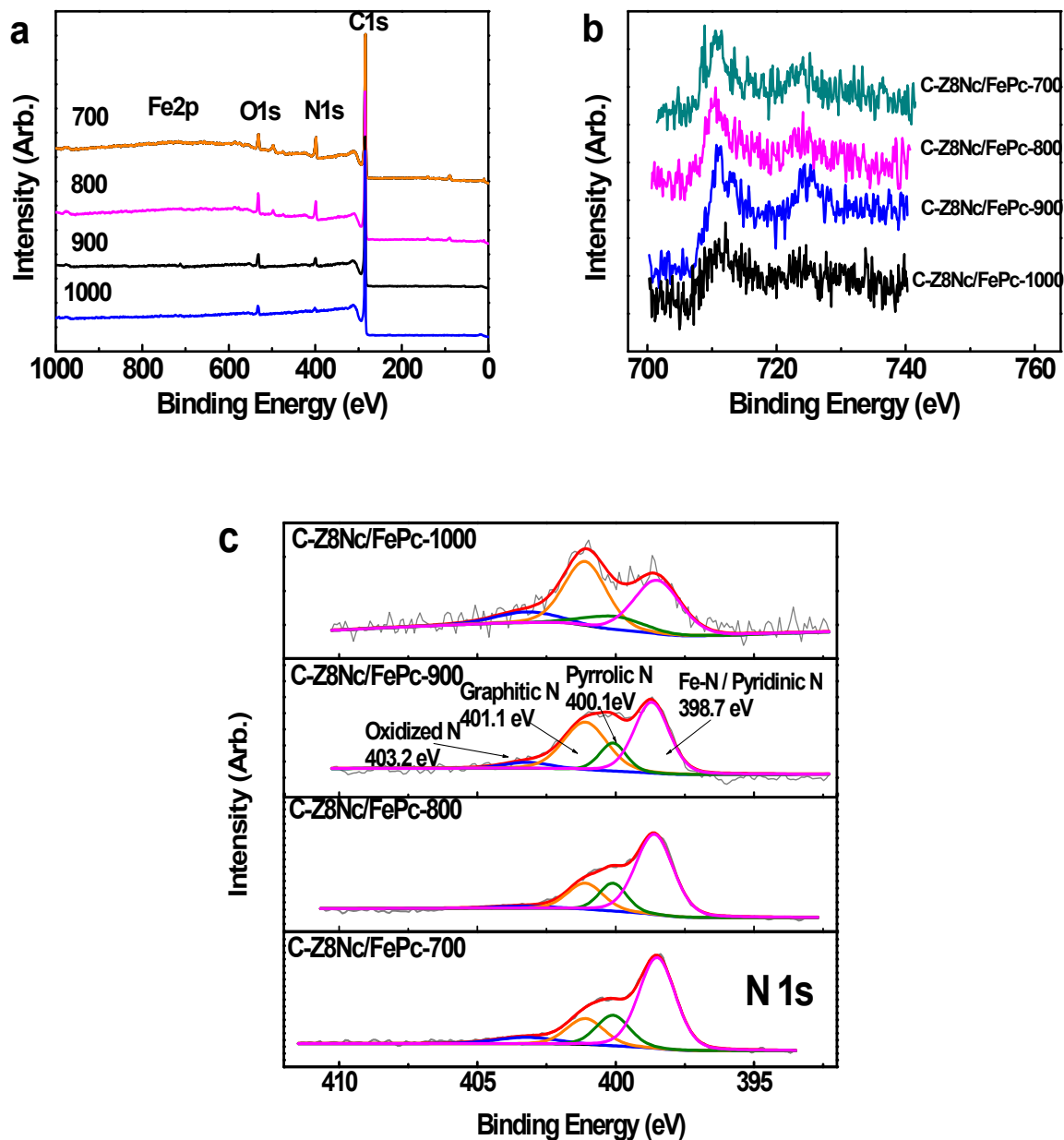
Fig. S11 (a) Survey XPS spectra, high-resolution (b) Fe2p and (c) N1s XPS spectra of C-Z8Nc/FePc obtained using different pyrolysis temperatures.
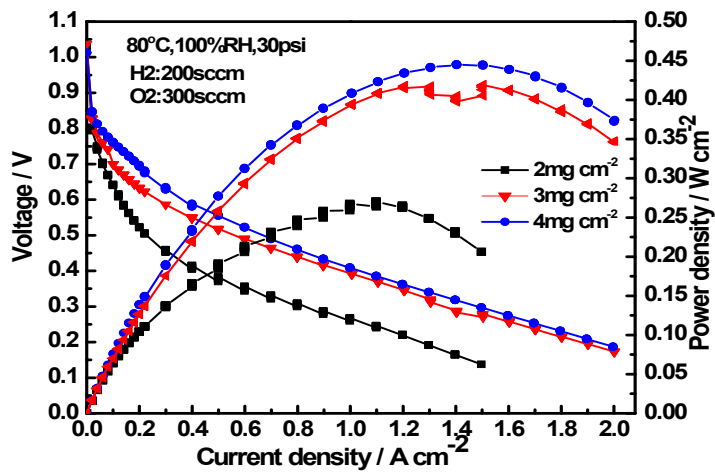
Fig. S12 Polarization plots of a single H_2-O_2 PEMFC with C-Z8Nc/FePc-900 as the cathode (loading:2-4mg cm^{-2}) and the Pt loading at anode was 0.2 mg cm^{-2}.

**Table S2.** ORR activities of typical reported NPM catalysts in acid solutions.

Catalyst	E_{onset} vs RHE (V)	$E_{1/2}$ vs RHE (V)	Electrolyte	Loading (mg cm^{-2})	References
C-Z8Nc/FePc-900	0.910	0.790	0.1 M HClO$_4$	0.510	This work
Fe$_3$C/NG-800	0.92	0.77	0.1 M HClO$_4$	0.400	[1]
Fe-C-PANI/NSA	0.86	0.73	0.1 M HClO$_4$	0.510	[2]
C700/950	0.915	0.811	0.5 M H$_2$SO$_4$	0.800	[3]
PpPD-Fe-C	0.826	0.718	0.5 M H$_2$SO$_4$	0.900	[4]
PFeTTPP-1000	0.93	0.76	0.1 M HClO$_4$	0.400	[5]
ZIF-67-900	0.85	0.71	0.5 M H$_2$SO$_4$	0.400	[6]
Zn(eIm)$_2$ TPIP	0.914	0.78	0.1 M HClO$_4$	0.400	[7]
VB12/Silica colloid	——	0.79	0.5 M H$_2$SO$_4$	0.600	[8]
FeCo-OMPC	1.00	0.851	0.1 M HClO$_4$	0.600	[9]

Table S3. ORR activities of typical reported NPM catalysts in alkaline solutions.

Catalyst	E_{onset} vs RHE (V)	$E_{1/2}$ vs RHE (V)	Electrolyte	Loading (mg cm^{-2})	References
C-Z8Nc/FePc-900	1.000	0.885	0.1M KOH	0.510	This work
Fe$_3$C/NG-800	0.92	0.77	0.1M KOH	0.400	[1]
CNPs	1.03	0.92	0.1M KOH	0.392	[10]
Fe$_3$C-GNRs	0.95	0.78	0.1M KOH	——	[11]
ZIF-67-900	0.91	0.85	0.1M KOH	0.400	[6]
Carbon-L	0.8610	0.6972	0.1M KOH	0.100	[12]
TTF-700	0.822	——	0.1M KOH	0.300	[13]
NOSC8-900	0.96	——	0.1M KOH	0.203	[14]
HNCS71	0.97	0.82	0.1M KOH	0.500	[15]
Co@Co3O4@C-CM	0.93	0.81	0.1M KOH	0.100	[16]
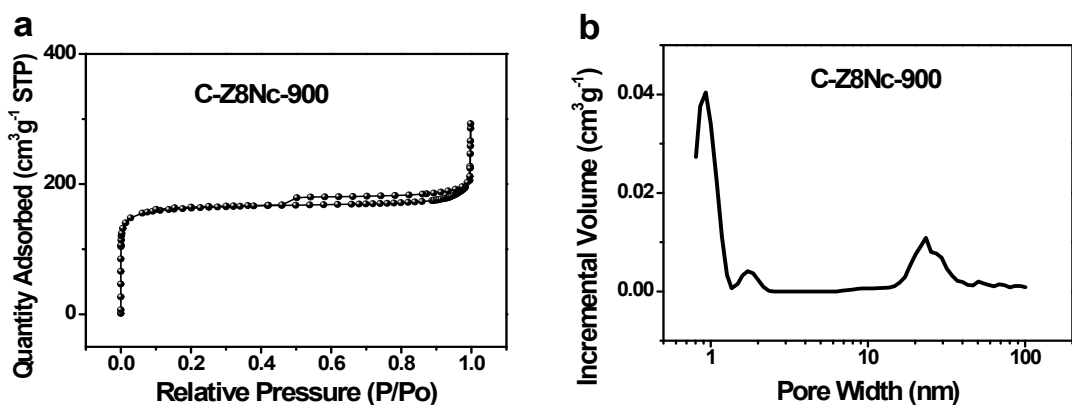
Fig. S13 N$_2$ adsorption and desorption isotherm and DFT pore size-distribution of C-Z8Nc-900.
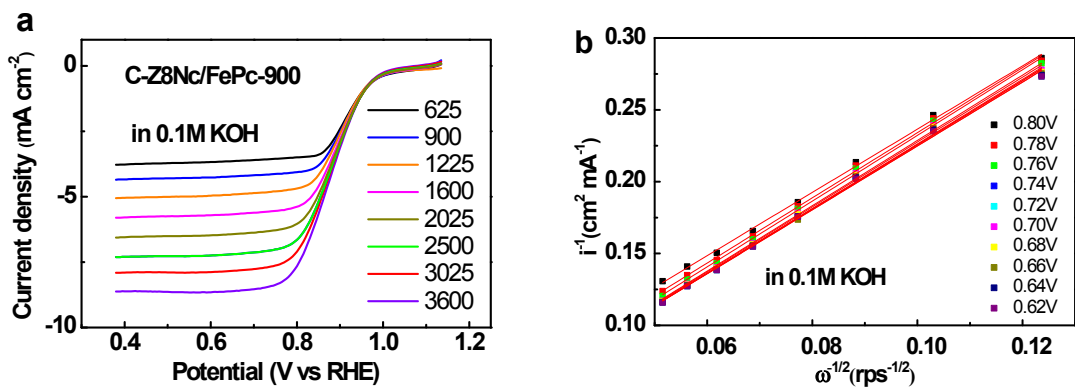
Fig. S14 (a) ORR curves of C-Z8Nc/FePc-900 obtained at different rotation rates in 0.1 M KOH; (b) K-L plots of i^{-1} versus $\omega^{-1/2}$ at different potentials on C-Z8Nc/FePc-900 in 0.1 M KOH.
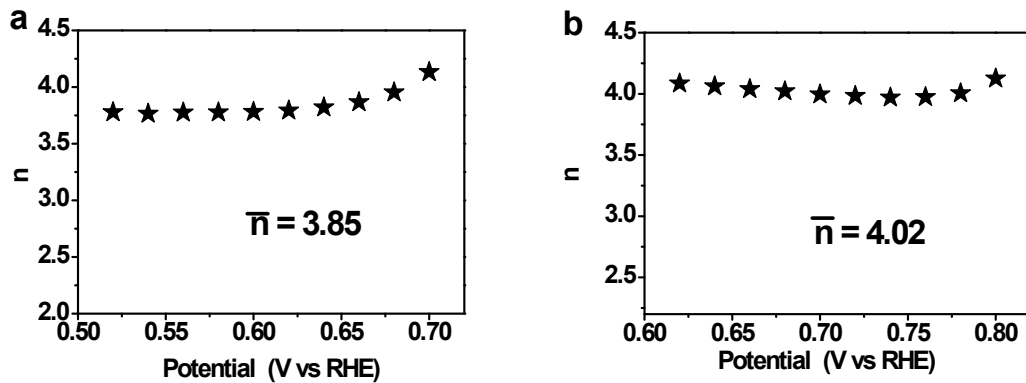
Fig. S15 Transferred electron numbers (a) in 0.1 M $HClO_4$, (b) in 0.1 M KOH.
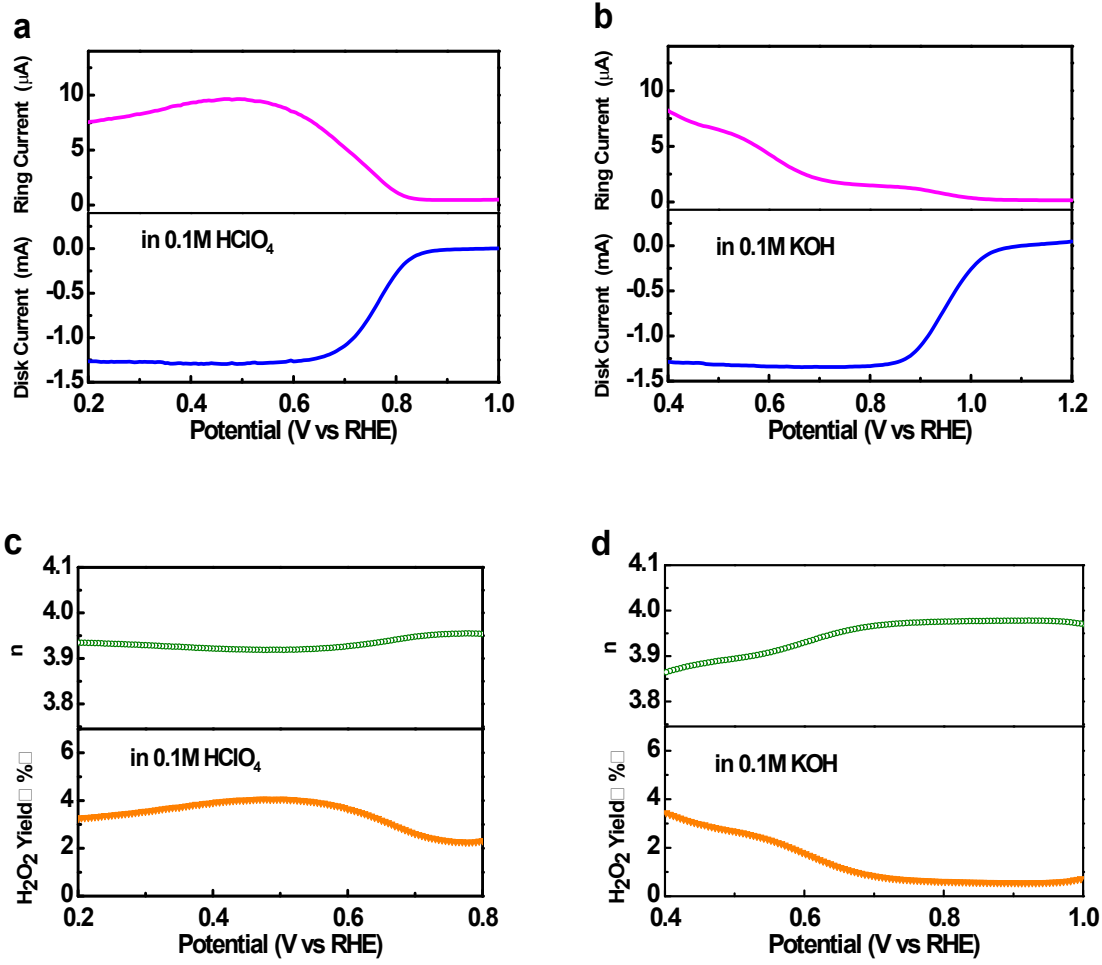
Fig. S16 RRDE measurement results in (a) 0.1 M HClO₄ and (b) 0.1 M KOH at a rotation rate of 1600 rpm; Peroxide yields and electron transfer numbers of C-Z8Nc/FePc-900 in (c) 0.1 M HClO₄ and (d) 0.1 M KOH calculated from the RRDE measurement results.
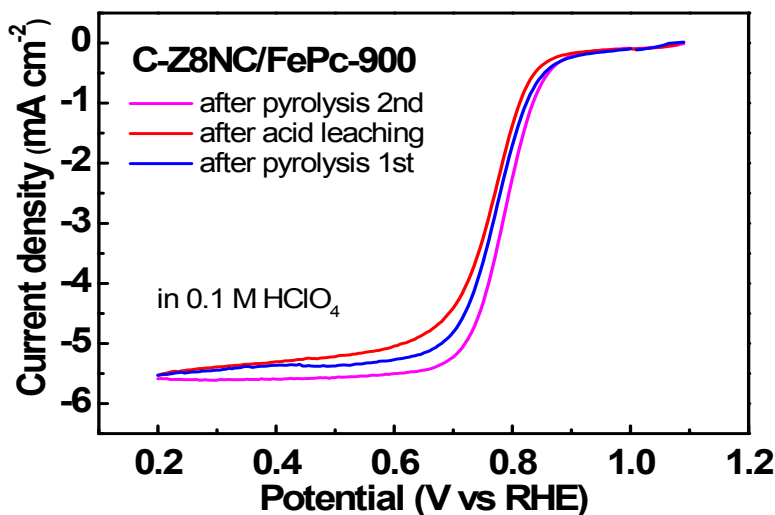
Fig. S17 ORR curves of C-Z8Nc/FePc-900 after the first pyrolysis, after acid leaching and after the second pyrolysis.

We further investigated the effect of Fe content in the precursors on the morphology of the materials. As shown in Fig. S18a-e, the materials prepared with Fe contents from 1 to 4 wt% in the precursors remained almost the same morphology, however, when the Fe content in the precursor reached 5 wt%, no hollow-core carbon can be observed, but only amorphous structure was obtained. We conducted several experiments using different amounts of iron in the precursors to investigate the effect of iron content on the ORR activity (Fig. S19). The ORR activity increased as the Fe contents in the precursors increased from 1 to 2 wt%, and decreased when the Fe contents in the precursors increased from 2 to 5 wt%. Actually, the final Fe contents in the catalysts are different from the initial Fe contents in the precursors. Therefore, we measured the final iron contents for these catalysts using ICP-AES and listed the results in Table S4. Our best catalyst C-Z8Nc/FePc-900 (prepared with 2 wt% Fe in the precursor) has final iron content of 3.21 wt%. We found that for this type of catalyst, 3.21 wt% Fe in the catalyst was enough to obtain the highest activity; further increasing iron content yielded inferior activities.
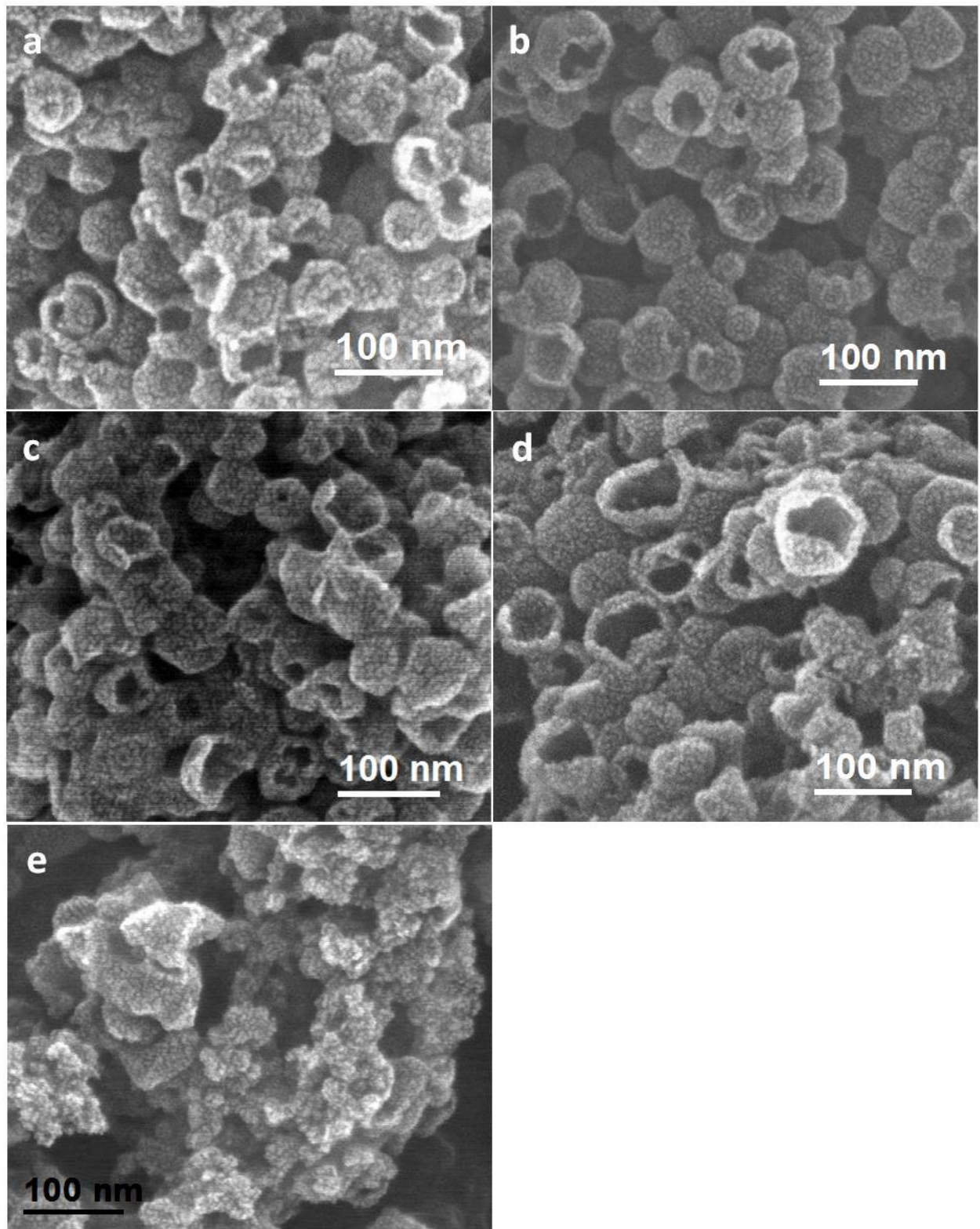
Fig. S18 SEM images of C-Z8Nc/FePc-900 with different Fe contents in the precursors (a) 1wt%, (b) 2wt%, (c) 3wt%, (d) 4wt%, (e) 5wt%.
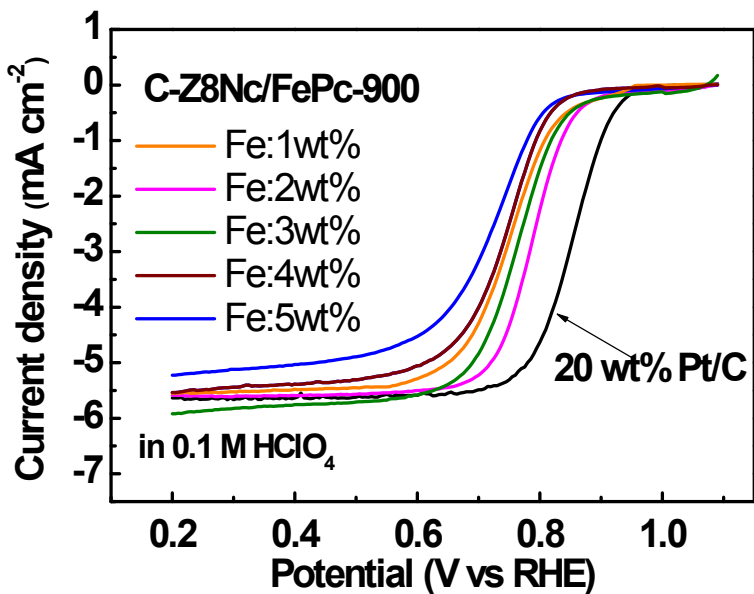
Fig. S19 ORR curves of C-Z8Nc/FePc-900 with different Fe contents in the precursors.

Table S4   Total mass of precursors, mass of Fe, Fe contents in precursors, total mass of final catalysts, mass of Fe, and Fe contents in final catalysts for the C-Z8Nc/FePc-900 with different Fe contents in precursors.

total mass of precursors (mg)	mass of Fe in precursors (mg)	Fe content in precursors (wt%)	total mass of final catalysts (mg)	mass of Fe in final catalysts (mg)	Fe content in final catalysts (wt%)
111.1	1.11	1	21.7	0.54	2.47
125.0	2.50	2	25.3	0.81	3.21
142.9	4.29	3	29.8	1.08	3.64
166.7	6.67	4	35.2	1.39	3.96
200.0	10.00	5	44.1	1.97	4.47

The Fe contents in the final catalysts were measured by ICP-AES.

In the acid leaching, H_2SO_4 is excess.

SUPPLEMENTARY REFERENCES:

1. M. Xiao, J. Zhu, L. Feng, C. Liu and W. Xing, *Adv. Mater.*, 2015, **27**, 2521-2527.

2. R. Zheng, Z. Mo, S. Liao, H. Song, Z. Fu and P. Huang, *Carbon*, 2014, **69**, 132-141.

3. F. Afsahi and S. Kaliaguine, *J. Mater. Chem. A*, 2014, **2**, 12270-12279.

4. Y. Zhu, B. Zhang, X. Liu, D.-W. Wang and D. S. Su, *Angew. Chem., Int. Ed.*, 2014, **53**, 10673-10677.

5. S. Yuan, J.-L. Shui, L. Grabstanowicz, C. Chen, S. Commet, B. Reprogle, T. Xu, L. Yu and D.-J. Liu, *Angew. Chem. Int. Ed.*, 2013, **52**, 8349-8353.

6. X. Wang, J. Zhou, H. Fu, W. Li, X. Fan, G. Xin, J. Zheng and X. Li, *J. Mater. Chem. A*, 2014, **2**, 14064-14070.

7. D. Zhao, J.-L. Shui, L. R. Grabstanowicz, C. Chen, S. M. Commet, T. Xu, J. Lu and D.-J. Liu, *Adv. Mater.*, 2014, **26**, 1093-1097.

8. H.-W. Liang, W. Wei, Z.-S. Wu, X. Feng and K. Muellen, *J. Am. Chem. Soc.*, 2013, **135**, 16002-16005.

9. J. Y. Cheon, T. Kim, Y. Choi, H. Y. Jeong, M. G. Kim, Y. J. Sa, J. Kim, Z. Lee, T.-H. Yang, K. Kwon, O. Terasaki, G.-G. Park, R. R. Adzic and S. H. Joo, *Sci. Rep.*, 2013, DOI: 10.1038/srep02715

10. S. Zhao, H. Yin, L. Du, L. He, K. Zhao, L. Chang, G. Yin, H. Zhao, S. Liu and Z. Tang, *ACS Nano*, 2014, **8**, 12660-12668.

11. X. Fan, Z. Peng, R. Ye, H. Zhou and X. Guo, *ACS Nano*, 2015, **9**, 7407-7418.

12. P. Zhang, F. Sun, Z. Xiang, Z. Shen, J. Yun and D. Cao, *Energy Environ. Sci.*, 2014, **7**, 442-450.

13. L. Hao, S. Zhang, R. Liu, J. Ning, G. Zhang and L. Zhi, *Adv. Mater.*, 2015, **27**, 3190-3195.

14. Y. Meng, D. Voiry, A. Goswami, X. Zou, X. Huang, M. Chhowalla, Z. Liu and T. Asefa, *J. Am. Chem. Soc.*, 2014, **136**, 13554-13557.

15. J. Sanetuntikul, T. Hang and S. Shanmugam, *Chem. Commun.*, 2014, **50**, 9473-9476.

16. X. Wei, Z. Ruqiang, A. Li and X. Dingguo, *Energy Environ. Sci.*, 2015, **8**, 568-576.